arXiv:1001.2627v1 [astro-ph.CO] 15 Jan 2010

Last Modified January 15, 2010

Stellar Mass Estimation Based on IRAC Photometry for *Spitzer* SWIRE-field Galaxies

Yi-Nan Zhu[1,2,3], Hong Wu[1,2], Hai-Ning Li[1,2,3], Chen Cao[4]

ABSTRACT

We analyze the feasibility to estimate the stellar mass of galaxies by mid-infrared luminosities based on a large sample of galaxies cross-identified from *Spitzer* SWIRE fields and SDSS spectrographic survey. We derived the formulae to calculate the stellar mass by using IRAC 3.6μm and 4.5μm luminosities. The mass-to-luminosity ratios of IRAC 3.6μm and 4.5μm luminosities are more sensitive to star formation history of galaxies than other factors, such as the intrinsic extinction, metallicity and star formation rate. To remove the affection from star formation history, we used g-r color to recalibrate the formulae and obtain a better result. It must be more careful to estimate the stellar mass of low metallicity galaxies using our formulae. Due to the emission from dust heated by hottest young stars, luminous infrared galaxies present higher IRAC 4.5 μm luminosity compared to IRAC 3.6 μm luminosity. For most of type-II AGNs, the nuclear activity can not enhance 3.6μm and 4.5μm luminosities compared with normal galaxies. The star formation in our AGN-hosting galaxies is also very weak, almost all of which are early-type galaxies.

Subject headings: galaxies: stellar content — galaxies:active — infrared: galaxies

---

[1] National Astronomical Observatories, Chinese Academy of Sciences, Beijing 100012, China; zyn@bao.ac.cn; hwu@bao.ac.cn; lhn@bao.ac.cn

[2] Key Laboratory of Optical Astronomy, National Astronomical Observatories, Chinese Academy of Sciences, Beijing 100012, China

[3] Graduate University, Chinese Academy of Sciences, Beijing 100039, China

[4] Institute of Space Science and Physics, Shandong University at Weihai, Weihai, Shandong 264209, China; ccao00@gmail.com

1. Introduction

It is important to obtain the mass of galaxies for understanding the evolution of the universe. We know that the dark matter halo contains most of mass, and can only be detected using the effect of gravitation. So generally, the total mass of galaxies could only be computed on the basis of kinematics of bright stars, clusters, or even satellite galaxies (e.g., Rogstad & Shostak 1972; Roberts & Rots 1973; Ostriker et al. 1974). However, due to the restriction from lower resolution and lower sensibility of telescopes for detecting the motion of celestial bodies in high redshift galaxies, these methods are just used for deriving general properties of nearby galaxies. Though the fraction of baryonic components in galaxies is relatively small, it could be detected and studied easily. Except the gas dominant galaxies, stars hold most of baryonic components in galaxies. Thus, to understand the correlation between the stellar mass and total mass is essential for studying the faint and distant galaxies. Therefore, it is necessary to seek some methods to estimate the stellar mass in galaxies.

If we know the mass-to-luminosity ratio of a galaxy, and assume an initial mass function (IMF), its stellar mass could also be estimated from the luminosity in corresponding wavelength (e.g., Bell & de Jong 2001; Portinari et al. 2004). Traditionally, mass-to-luminosity ratios could be derived by fitting photometric colors or spectra with models. Most of baryonic components are trapped in low mass stars, which dominate the output of galaxies in longer wavelength range compared to the massive ones. At the same time, the short life scale of massive stars and heavy extinction in relatively short wavelength ranges restrict us to use them to detect the bulk of galactic stellar masses. Hence, less affected by other factors, such as metallicity, star formation rate (SFR) and star formation history (SFH), luminosities in relatively longer wavelength (for example, near-infrared (NIR) band), are ideal tracers of the stellar mass (e.g., Cole et al. 2001; Kochanek et al. 2001). The K band luminosity distribution of distant galaxies was discussed in support of the hierarchical picture by Kauffmann & Charlot (1998). The main uncertainty in the inferred stellar masses arises from the age of the stellar population (Rix & Rieke 1993), similar to the results calculated by optical luminosities (Bell et al. 2005). The discrepancy among stellar masses derived from various methods has been found (e.g., Drory et al. 2004). For example, the uncertainty of the stellar mass estimated by K-band luminosity alone has been discussed by Brinchmann et al (2000). Kannappan & Gawiser (2007) compared many estimation methods for local galaxies and also showed the differences (the factors up to 2) among them.

Except for above methods, the stellar mass could also be directly calculated using mid-infrared (MIR) luminosities in 3-5μm, since emissions from the photosphere of old stars dominate the output of galaxies in this wavelength range. At the same time, the extinction and reddening in this range are clearly weak. But using these emissions to study the universe was prevented because of the absorption of atmosphere until the onset of space infrared observations. *Spitzer Space Telescope* (Werner et al. 2004) is a very useful facility to help us to study the MIR to far-infrared (FIR) emission properties of galaxies. The two detectors in the shorter wavelength bands (3.6μm and 4.5μm) of *Spitzer* Infrared Array Camera (IRAC; Fazio et al. 2004) could be treated as stellar mass tracers of nearby galaxies, although some disturbances may exist, such as the continuum from hot dust or spectral features from the polycyclic aromatic hydrocarbons (PAHs; Léger & Puget 1984; Puget & Léger 1989; Draine 2003; Wu et al. 2005). Using about 150 local galaxies, Li et al. (2007) showed that there truly existed tight correlations between the K-corrected 3.6μm luminosities and the stellar mass based on the Bell et al.'s (2003) formula.

In this paper, we want to derive the stellar mass formulae using IRAC 3.6 and 4.5 μm luminosities based on the observation of *Spitzer* and Sloan Digital Sky Survey (SDSS; York et al. 2000). The *Spitzer* Wide-area Infrared Extragalactic Survey (SWIRE; Lonsdale et al. 2003), with a total field of $\sim$49 deg^2, is the largest extragalactic survey program among the six *Spitzer* cycle-1 Legacy Programs, and provides us a best opportunity to establish such correlations.

The structure of the paper is as follows. We describe the construction of our sample and the referenced stellar mass in §2. The major results of the MIR stellar mass estimations are presented in §3. Discussion and summary are given in §4 and §5. Throughout this paper, we adopt a ΛCDM cosmology with $\Omega_{\rm m} = 0.3$, $\Omega_\Lambda = 0.7$ and $H_0 = 70\,{\rm km\,s^{-1}Mpc^{-1}}$.

2. The Sample and Reference Stellar Mass

The optical spectral sample galaxies are selected from the Sloan Digital Sky Survey (SDSS; York et al. 2000) main galaxy sample (Strauss et al. 2002), with r-band Petrosian magnitudes lower than 17.77 mag. A total 15 deg^2 of SDSS sky matches the three northern *Spitzer* SWIRE fields. The derived data from SDSS DR7, including the stellar mass, was supplied by The Max-Planck-Institute for Astrophysics (MPA) and the Johns Hopkins University (JHU) in their archives [1]. Compared with former data releases, such as DR4, some galaxies were excluded in DR7 due to new restricts on the detected sources before publication by MPA/JHU. The stellar mass derived from fitting photometries with population synthesis models was treated as reference. The foreground extinction in all the five SDSS bands were corrected by subtracting the extinction values presented in the SDSS catalog. The IDL code by Blanton (version tag v4_1_4) was used to calculate the K-correction. The method and the SED used in this code were described in details by Blanton et al. (2003) and Blanton & Roweis (2007).

---

[1] http://www.mpa-garching.mpg.de/SDSS/DR7

The IRAC four bands (3.6, 4.5, 5.8 and 8.0 μm) images were mosaicked from the Basic Calibrated Data (BCD; acquired from the *Spitzer* Sciences Center) after the flat-field corrections, dark subtraction, linearity and flux calibrations (Fazio et al. 2004; Huang et al. 2004), with the final pixel scale of $0.6''$ (Wu et al. 2005; Cao & Wu 2007; Cao et al. 2008). The MIPS 24μm images were mosaicked as the same way but with a pixel scale of $1.225''$ (Wen et al. 2007; Cao & Wu 2007; Wu et al. 2007). Based on the catalogs of the Two Micron All Sky Survey (2MASS; Skrutskie et al. 1997; Cutri et al. 2003), we enhanced the accuracy of the astrometric calibration of $0.1''$ in all five bands. The final IRAC and MIPS 24 μm flux has calibration uncertainties less than 10% (Rieke et al. 2004). Then we matched these MIR sources with the above SDSS sample galaxies with a cross radius of $2''$. For the purpose of this work, the sources with both IRAC 3.6μm and 4.5μm detections were selected. The basic sample contains 1454 objects. For all these sources, a set of Spectral Energy Distribution (SED) (Huang et al. 2007) was used to perform K-correction in IRAC 3.6μm and 4.5μm bands.

Only part of the galaxies (total is 659) have been mapped by $2MASS$. The Extended Source Catalog (XSC) was download from the archives of Infrared Processing and Analysis Center [$IPAC$] [2] and matched with the above sample with a cross radius of $2''$. The K-correction for $2MASS$ NIR band flux was also based on the IDL code by Blanton et al. (2003) and Blanton & Roweis (2007). The difference in $K_{\rm s}$ band between Vega magnitude which was used by $2MASS$ catalogs and AB magnitude is 1.84 (Finlator et al. 2000). And a factor of 5.12 (Finlator et al. 2000; Binney & Merrifield 1998)was used as the $K_{\rm s}$ band solar absolute magnitude.

2.1. Spectral Classification

For all the 1454 galaxies, 68 with positive Hα equivalent width were classified as absorption line galaxies, while the rest 1386 were classified as emission line galaxies. Futhermore, emission line galaxies with detected Hα, Hβ, [OIII], [NII] emission lines were selected, and optical spectral classifications were carried out on these 1152 galaxies, adopting the traditional BPT diagnostic diagram: [NII]/Hα versus [OIII]/Hβ (Baldwin et al. 1981; Veilleux & Osterbrock 1987), as shown in Figure 1. The dashed curve is from Kauffmann et al. (2003b) and the dotted curve is from Kewley et al. (2001). Objects located below the dashed curve were classified as star-forming galaxies; those between these two lines were classified as composite (starburst + AGN) galaxies (Kewley et al. 2006; Wu et al. 1998); while those above the dotted line were classified as narrow-line AGNs. Therefore, the final sample contains 1220 galaxies, including 561 star-forming galaxies, 292 composites, 299 narrow-line AGNs, and 68 absorption line galaxies, and 544 of this final sample have the $2MASS$ $K_{\rm s}$ band flux.

---

[2] http://irsa.ipac.caltech.edu/

Wu et al. (2007) presented an equation to compute d_{AGN} to represent AGN activities, defined as the distance of an AGN from its position (x_p,y_p) in dex in the traditionally line-diagnostic diagram [OIII]/Hβ versus [NII]/Hα to the Kewley et al. (2001)'s curve along the parallel of the best linear fitting of 27 AGNs. This is quite similar to the star-forming distance defined by Kewley et al. (2006) in the diagnostic diagram [OIII]/Hβ versus [OI]/Hα or [SII]/Hα. Here, we also use this formula to quantify AGN activities (see the orange solid line in Figure 1 as an example). In Figure 1, the two dotted-dashed lines above the dotted curve marked the boundaries that were used by Wu et al. (2007). Only sources whose EW(Hβ) were less than -5 were selected by Wu et al. (2007). But in this work, we did not use this limit to reduce those sources with smaller values of EW(Hβ), such as LINERs. Therefore, many AGNs appeared outside the right boundary in Figure 1.

2.2. Define Referenced Stellar Mass

The thermally pulsing asymptotic giant branch (TP-AGB) could dominate the output of galaxies at some evolutionary phases (Maraston et al. 2006; Bruzual 2007). But lots of evolutionary tracks used in stellar population synthesis models did not consider the effect from TP-AGB. So there must exist bias for the derived stellar mass when comparing observations with those models. For example, for young template models (with ages less than 2 Gyr), both Maraston et al. (2006) and Bruzual (2007) have concluded that galactic stellar masses calculated with an improved treatment of TP-AGB stars are roughly 50 to 60 per cent lower. Hence, due to the lower effective surface temperature of TP-AGB, referenced stellar mass derived from optical observations could avoid the emission of TP-AGB.

The referenced stellar mass used in this work was provided by MPA/JHU in their archive [3]. They derived stellar masses from fitting photometries (Salim et al. 2007) and spectral features (Gallazzi et al. 2005; Kauffmann et al. 2003a) with a large grid of models from BC03 (Bruzual & Charlot 2003) spanning a large range in SFH. The stellar mass derived using SDSS photometries could avoid the aperture effect which should be considered when fitting spectral features, since only a part of region of the observed object was covered by SDSS spectral fiber with $3''$ diameter. For about eighteen thousand galaxies randomly selected from MPA SDSS DR4 Sample, the stellar masses derived from photometries and spectral indices fits were compared and shown in Figure 2(a). We found a good correlation between them.

---

[3] http://www.mpa-garching.mpg.de/SDSS/

If the luminosity in some wavelength ranges could be obtained, we can estimate the stellar mass by assuming the mass-to-luminosity ratio in corresponding wavelength range. Bell et al. (2003) presented the relationship between various optical colors and mass-to-luminosity ratios. In Figure 2(b), we compared the referenced stellar mass with those computed based on the equation by Bell et al. (2003). Here, to correct the 'diet Salpeter' IMF (Bell et al. 2003) to the normal Salpeter (Salpeter 1955) IMF, we added a factor of 0.15 (Bell et al. 2003) to the stellar mass calculated by using rest-frame g-r color and r band model magnitude. And a factor of 4.67 (Bell et al. 2003) was treated as the r band solar absolute magnitude (note there is a difference with a factor of 0.09 against the value used by Blanton et al. (2003)). For the stellar mass derived from the equations of Bell et al. (2003), there is a systematical overestimation with factor of about $0.2-0.6$ dex, and such discrepancy is more obvious for a galaxy with lower stellar mass. This trend is more clear in Figure 3. The disagreement is more obvious for lower stellar mass and bluer galaxies than higher stellar mass and redder ones, which is similar to the results supplied by of Kannappan & Gawiser (2007) who found that large discrepancy existed between their reference stellar mass and the one derived from Bell et al.'s (2003) correlations, with factors in the range of 2 to 5.

2.3. Sample Distribution

The distributions of the SDSS B-band absolute magnitude ($\mathrm{M_B}$), redshift, referenced stellar mass and r band concentration parameters of star-forming galaxies, composite galaxies, AGNs and absorption line galaxies are shown in Figure 4. Here, $\mathrm{M_B}$ were calculated from the SDSS g and r-band model magnitudes according to Smith et al. (2002). Most of the galaxies, especially for composites, AGNs and absorption line galaxies, have $\mathrm{M_B}$ brighter than -18 mag, which usually is regarded as the boundary to distinguish with dwarf galaxies (Thuan & Martin 1981). Few galaxies have redshift larger than 0.15. Herce, most of the galaxies in our sample are local ones. The star-forming galaxies have lower stellar mass than the others in Figure 4(c). The morphology of galaxies was represented by r band concentration parameters ($R50/R90$), which defined as ratio of two radii containing 50% and 90% of the Petrosian r band luminosity. The values of $R50/R90$ are smaller for early-type galaxies than those of late-type galaxies. According the distributions of four different spectral type galaxies in Figure 4(d), we found that the morphologies of the composite galaxies, AGNs and absorption line galaxies are similar, but those of star-forming galaxies are later type. Therefore, on the basis of above discussions, we find that low luminous dwarf early-type galaxies are scarce in this sample.

3. Result: Stellar Mass Estimated by MIR luminosities

A lot of factors could effect the stellar mass estimations. Therefore, good stellar mass tracers should be insensitive to these factors. Figure 5 show the correlations between mass-to-luminosity ratios of $2MASS$ $K_{\rm s}$ band and two MIR bands luminosities and various factors. The $K_{\rm s}$ luminosity was proved to be an ideal stellar mass tracer. Figure 5(a1, a2, a3) present the effect of EW(Hα) on the mass-to-luminosity ratios. EW(Hα) is Hα equivalent width and could be regarded as the representative of SFH (Kennicutt 1998). The concentration parameters ($R50/R90$) in Figure 5(b1, b2, b3) represent the morphology of galaxies. The effect of color excess E(B-V) on the mass-to-luminosity ratios is illustrated in Figure 5(c1, c2, c3). E(B-V) is for the intrinsic extinction and calculated from Balmer decrement $F_{\rm H\alpha}/F_{\rm H\beta}$ (Calzetti 2001). Thus only the emission line galaxies are plotted here. In Figure 5(d1, d2, d3), the oxygen abundance is used to represent the metallicity of star-forming galaxies (Kauffmann et al. 2003a). The oxygen abundances of ISM were provided by Tremonti et al. (2004), which computed the abundances by fitting serial spectral features from SDSS observational spectra to models. The effect of AGN activities is shown in Figure 5(e1, e2, e3) by using d_{AGN} to represent AGN activities as like Wu et al. (2007). Only AGNs located in between the two boundaries defined by Wu et al. (2007) were adopted. We should note, except the concentration parameters, all above factors are derived from the spectral features in central regions covered by SDSS fibers with $3''$ diameter. For the correlations between M/L(3.6μm) and the five factors (EW(Hα), $R50/R90$, E(B-V), oxygen abundance, d_{AGN}), the Spearman Rank-order correlation analysis coefficients are 0.74, 0.58, 0.15, 0.45 and 0.01, respectively; while for the correlations between M/L(4.5μm) and the five factors (bottom five panels in Figure 5),the Spearman Rank-order correlation analysis coefficients are 0.77, 0.58, 0.10, 0.36 and 0.01, respectively. Hence, it is clear that the M/L(3.6μm) and M/L(4.5μm) are more sensitive to the EW(Hα), morphology and metallicity of galaxies. The value of the EW(Hα) represents SFH for galaxies without strong nuclear activities, while the morphology and metallicity are sensitive to the nowaday SFR other than the SFH.

In order to derive the formulae to estimate stellar masses using these three band luminosities, we present the correlations between them and stellar masses for all the galaxies in our sample firstly. The $K_{\rm s}$ band, 3.6μm and 4.5μm bands luminosities are plotted against stellar masses in Figure 6. The stellar masses are the referenced one described in §2.2. These galaxies show good correlations between the three band luminosities and stellar masses. The best nonlinear and linear fits are shown as solid and dotted lines in Figure 6, and the fitting parameters are listed in Table 1. Here, the best nonlinear fits are obtained by using two-variable regression. Similar to Li07, we can derive star mass formulae based on the non-linear correlations:

$$Log_{10}\ M_{\star,ref} = (-1.60 \pm 0.05) + (1.12 \pm 0.02) \times Log_{10}\ \nu L_{\nu}[K_{\rm s}] \tag{1}$$

$$Log_{10}\ M_{\star,ref} = (-0.79 \pm 0.03) + (1.19 \pm 0.01) \times Log_{10}\ \nu L_{\nu}[3.6\mu m] \tag{2}$$

$$Log_{10}\ M_{\star,ref} = (-0.25 \pm 0.03) + (1.15 \pm 0.01) \times Log_{10}\ \nu L_{\nu}[4.5\mu m] \tag{3}$$

The correlations between two IRAC band luminosities and referenced stellar mass are as tight as that between the $K_{\rm s}$ band luminosities and referenced stellar masses. The fitting residuals' standard deviations and the Spearman Rank-order correlation analysis coefficients of the correlations of 3.6μm and 4.5μm luminosities with stellar masses are 0.11 and 0.12, 0.96 and 0.95, respectively. The dashed line shown in Figure 6(b) represents the non-linear fits for local luminous galaxies in the northern *Spitzer* SWIRE fields obtained by Li et al. (2007). Comparing the best non-linear fits in this work with that of Li et al. (2007), an obvious downward shift exists, especially for the non-luminous ones. For example, for galaxies with 3.6μm luminosity of $10^9 L_{\odot}$, the stellar mass estimated from formula (2) would be about 0.5 dex lower than the result from corresponding formula in Li et al. (2007). The shift could be due to fact that different stellar mass references (Figure 2) are used in these two works.

Above analysis ignored the effect by different SFH. In fact, there is such effect, at least for star-forming galaxies illustrated in Figure 5(a1, a2, a3), which showed the correlations between the EW(Hα) and mass-to-luminosity ratios of $K_{\rm s}$ band, 3.6μm and 4.5μm luminosities. The SFH could also be represented with the g-r color indicated by both Bell & de Jong (2001) and Kauffmann et al. (2003a), which was also proved an effective method to estimate the stellar mass by Gallazzi & Bell (2009). Figure 7 shows the correlation between g-r color and the EW(Hα) of our sample galaxies. There exists obvious anti-correlation between -EW(Hα) and g-r color. Therefore, we calibrate the correlations between mass-to-luminosity ratios and g-r color. Panels in Figure 8 show the correlations between various mass-to-luminosity ratios and g-r colors. Here, SDSS model magnitudes are used, and the foreground extinction and redshift have been corrected.

These mass-to-luminosity ratios that are shown in Figure 8 are not constantly following the changing of color. From these four panels, we find out that redder galaxies tend to have larger mass-to-luminosity ratios. Using the two-variable regression, we obtain the best non-linear fits illustrated as solid lines in four panels of Figure 8 and the fitting parameters are listed in Table 2. According to these correlations, we derive the formulae to estimate the stellar mass:

$$Log_{10}\frac{M_{\star,ref}}{\nu L_{\nu}(r)} = (-0.81 \pm 0.01) + (1.47 \pm 0.01) \times (g - r) \tag{4}$$

$$Log_{10}\frac{M_{\star,ref}}{\nu L_{\nu}(K_{\rm s})} = (-1.29 \pm 0.05) + (1.42 \pm 0.06) \times (g - r) \tag{5}$$

$$Log_{10}\frac{M_{\star,ref}}{\nu L_{\nu}(3.6)} = (0.23 \pm 0.01) + (1.14 \pm 0.01) \times (g - r) \tag{6}$$

$$Log_{10}\frac{M_{\star,ref}}{\nu L_{\nu}(4.5)} = (0.39 \pm 0.01) + (1.17 \pm 0.02) \times (g - r) \tag{7}$$

The dotted-dashed line in Figure 8(a) is the respective line by Bell et al. (2003) (see their Table.7, Fig.6 and Fig.20). The slope of our fit of M/L(r) vs. g-r color is much deeper than that of Bell et al. (2003). Gallazzi & Bell (2009) also found similar discrepancy. One possible explanation is that different evolutionary population synthesis models have been used to derive standard stellar mass. The correlation between M/L(r) and g-r color is the tightest one, with the Spearman Rank-order correlation analysis coefficients of 0.97 and the fitting residuals' standard deviations of 0.03. The correlations of M/L(3.6μm) and M/L(4.5μm) with g-r color are also tight, with fitting residuals' standard deviations of 0.05 and 0.06, and the Spearman Rank-order correlation analysis coefficients of 0.83 and 0.80, respectively. The scatter in Figure 8(a) is apparently much smaller than those in other panels, but the slope of the correlation between M/L(r) and g-r color for red galaxies is a little shallower than the slope for blue ones. This variation is also suggested in Kauffmann et al. (2003a) based on about 100,000 SDSS galaxies. Besides SFH, some other factors could possibly account for this slope variation, too. This variation can not be found in other panels in Figure 8. If the variations exist in Figure 8(b, c, d), we can not clearly see them due to large scatters. The distribution of mass ratios of derived stellar mass and the reference one in Figure 9 show that the stellar masses derived by using Eq.6 and 7 are much tighter than the respective ones from Eq.2 and 3.

4. Discussion

4.1. Comparion with $K_{\rm s}$ band

$K_{\rm s}$ band luminosity was often used to derive stellar masses of galaxies. From Figure 5, Figure 6 and Figure 8, we find that IRAC 3.6μm and 4.5μm luminosities are also good stellar mass tracers compared with $K_{\rm s}$ band luminosity, because the radiation in all these bands was dominated by old stellar populations. Additionally, for the same sky area, the effect of extinctions in IRAC 3.6μm and 4.5μm photometries is absolutely weaker than that in 2*MASS* $K_{\rm s}$ band (e.g., Gao et al. 2009). There has been very few calibrations between stellar masses and 3μm to 5μm emissions. One major reason is the limit of the weak transmissions of earth's atmosphere in this wavelength range. Now, the progress of space astronomy make us capable to observe the MIR sky directly.

Bell et al. (2003) indicated that the dispersion of blue galaxies was diffused in the M/L($K_{\rm s}$) vs. B-R plane (their Figure 20). And the fitting slope was shallower for red galaxies compared to the blue ones. Using modified broad band Johnson photometry correlation, Kannappan & Gawiser (2007) also found similar variation of the slope. The transformation point of the slope of Kannappan & Gawiser (2007) was 1.2 in Johnson optical color B-R, which corresponded to a SDSS g-r color of 0.55 based on the transformation methods supplied by Fukugita et al. (1996). In their work, the slope of the correlation of M/L($K_{\rm s}$) vs. B-R was 0.5 for blue galaxies with B-R color less than 1.2, while for the red galaxies with B-the corresponding slope was 0.34. Bell et al. (2003) found out that the reason for diffused dispersion and transformation of slope was the difference of metallicity of blue galaxies. For two galaxies with same in M/L($K_{\rm s}$), the one with lower metallicity must be bluer than the higher metallicity one optical colors. However we do not find such phenomena in other three panels(Figure 8(b,c,d)), because of the lack of low metallicity galaxies in this sample, or the larger dispersion. Therefore, it must be more careful when estimating stellar masses of low metallicity galaxies using NIR or MIR luminosities. We will investigate their properties in more details in future.

4.2. Effect of Star Formation

Besides the EW(Hα), mass-to-luminosity ratios of two MIR luminosities are also sensitive to the concentration parameters which could be seen in Figure 5. Figure 10 shows the correlations between stellar mass ratios (the stellar mass derived from above formulae divided by the reference stellar mass) and morphology ($R50/R90$). The derived stellar masses in Figure 10(a, b) base on nonlinear fits of 3.6μm and 4.5μm luminosities (with superscript 'A') vs. reference stellar masses (Eq.2 and 3); while those in Figure 10(c, d) base on nonlinear fits of M/L(3.6μm) and M/L(4.5μm) vs. g-r color (Eq.6 and 7) (with superscript 'B'). We find out that the obvious discrepancies of derived stellar masses of galaxies with different morphologies in Figure 10(a, b) would overestimate the stellar masses of the late-type galaxies compared to the early-type ones; while the ratios keep nearly constant in Figure 10(c, d). SFH could account for the discrepancies in Figure 10(a, b) when comparing the slopes of two upper panels and two bottom panels. Except for SFH, SFR may be another factor resulting in overestimations of stellar masses for late-type galaxies. Galaxies with different morphologies have different SFRs. There are more new stars born in late-type galaxies than in early-type ones (Li et al. 2007). SFR could relate with the values of intrinsic extinction and metallicity as shown in Figure 5. Hence, it is necessary to check SFR on our stellar mass formulae.

Panels in Figure 11 are similar to those in Figure 10, just replacing r band concentration parameters by 24μm luminosities of galaxies. Same as Figure 10, stellar masses in two upper panels (Figure 11(a, b)) are derived by nonlinear fits of 3.6μm and 4.5μm luminosities (Eq.2 and 3), while those in bottom panels (Figure 11(c, d)) based on the nonlinear fits of M/L(3.6μm) and M/L(4.5μm) vs. g-r color (Eq.6 and 7). A template SED of a normal HII galaxy NGC 3351 (from SINGS; (Kennicutt et al. 2003)) was used to perform K-correction for the 24μm band for all the sample galaxies with 24μm detection. Figure 11 shows that Eq.2 and 3 would overestimate the stellar mass for galaxies with higher 24μm luminosities. The 24μm luminosity was proved to be a good SFR tracer by *Spitzer* observations (Wu et al. 2005; Calzetti et al. 2005, 2007; Zhu et al. 2008). Therefore, Eq.2 and 3 are available for galaxies with lower star-forming activities. While Figure 11(c, d) are almost flat. Thus, the Eq.6 and 7 are not quite sensitive to SFR or morphology (Figure 10).

In Figure 11, there are three outliers which are marked with red crosses. The one with number '3' is an AGN, which will be discussed in next subsection. Other two sources are star-forming galaxies with apparent features of interactions or mergers in SDSS images. The one with number '1' is a dwarf star-forming galaxies, with low metallicity of 7.93 and very large 24μm-to-3.6μm flux ratio. The one with number '2' is a luminous star-forming galaxies with strong PAH emissions in IRAC 8μm band. Both of them have very blue g-r color. Actually, they are the only two galaxies with g-r color less than 0.1 in Figure 8. Additionally, the stellar mass of '2' derived by using SDSS photometries and spectral indices are apparently different. Therefore, it is hard to define which one is the best estimator. The stellar mass estimated using photometries is about 1 dex less than the one estimated by spectral indices. For '1' and '3', there are no stellar masses values derived by spectral indices.

Apart from emission directly from the photosphere of old red stars, the continuum from very small dust heated by hot stars, even some broad emission features (Gillett et al. 1973; Willner et al. 1977) which were indicated to be from PAHs (Wen et al. 2007; Cao & Wu 2007), could increase the MIR luminosity of a galaxy. The dust emission dominates radiation of star-forming galaxies in the wavelength range beyond 5μm, but could also enhance the 4.5μm flux(Helou et al. 2004). To evaluate such effect, the 4.5μm-to-3.6μm flux ratio is plotted against the 24μm luminosity in Figure 12. The three outliers in Figure 11 were marked with red crosses. The blue boxes are the AGNs. There are some AGNs with very high 4.5μm-to-3.6μm luminosity ratios marked with red boxes. Except these outliers, we find a correlation between 4.5μm-to-3.6μm luminosity ratio and star formation for most of sources. Because the 24μm luminosity is the tracer of SFR, this correlation may be due to the dust emissions in the 4.5μm band. With the assumption that the entire IRAC 3.6μm band luminosity is from the stellar emission, a factor of 0.596 (Helou et al. 2004) was used to scale the stellar continuum of 3.6μm to that of 4.5μm based on *Starburst99* synthesis model (Leitherer et al. 1999) with the solar metallicity and a Salpeter initial mass function (IMF) between 0.1 and 120 $M_{\odot}$. This factor is similar to that derived from the observed SED of early type galaxies by Wu et al. (2005). The factor of 0.596 is plotted with dashed line in Figure 12. If this factor is available for all star-forming galaxies, we could estimate the dust emission fraction based on the correlations between 24μm and total-infrared (TIR) luminosities(Zhu et al. 2008), e.g., for luminous infrared galaxies with TIR luminosity of $10^{11}L_{\odot}$, about 30% flux at rest-frame 4.5μm is from dust emission. Therefore, compared to the 4.5μm emission, IRAC 3.6μm emission is a better stellar mass tracer. This is also supported by the much tighter correlation between 3.6μm and stellar masses in Table 1 and 2.

4.3. Effect of AGNs

Due to the powerful UV emissions from AGNs, the dust surrounding them could be heated by central monsters and then re-radiate in IR range (see, e.g, Bell et al. 2005; Pérez-González et al. 2006; Elbaz et al. 2007; Daddi et al. 2007). Higher MIR-to-Hα/MIR-to-UV luminosity ratios were found by previous works based on *Spitzer* observations (Wu et al. 2007; Li et al. 2007; Zhu et al. 2008). So we want to know whether the energy from AGNs could strengthen the 3.6μm and 4.5μm emissions. Figure 13 shows the correlations between stellar mass ratios and AGN activities. Here, just the AGNs located inside the two boundaries defined by Wu et al. (2007) are adopted. Kauffmann et al. (2003b) found that the contribution from AGN light to the optical continuum was much weaker compared to from starburst. Thus, ignoring the effect of AGN emission on the estimation of referenced stellar mass would be reasonable. Red boxes represent the respective AGNs in Figure 12 with 4.5μm-to-3.6μm flux ratio large than 0.9. According to Wen et al. (2007), we know that AGNs with very high 4.5μm-to-3.6μm ratios may be QSOs. In Figure 13, except those scatters, the stellar mass derived from MIR luminosities keep constant with increasing d_{AGN}, while Figure 5(e2, e3) show that AGN activities can not disturb mass-to-luminosity ratio for AGN-hosting galaxies, even at 4.5μm(Figure 14). Therefore, there seems no confirmed non-thermal radiations or dust emissions heated by AGNs in IRAC 3.6μm and 4.5μm detections. Because all the sources here are type-II AGNs, the powerful intrinsic extinction of dust torus of narrow line AGNs could be another explanation for non-detection of AGNs in 3.6μm and 4.5μm in our sample. The absence of AGN emissions at 3.6μm and 4.5μm also indicate that the stellar mass formulae based on 3.6μm and 4.5μm luminosities are applicate to most AGN-hosting galaxies.

Figure 4 present the distributions of absolute B-band magnitudes, reference stellar masses and r band concentration parameters. The distributions in Figure 4 of composite galaxies and AGNs are strikingly different from those of star-forming galaxies, but similar to absorption line galaxies. These results indicate that AGNs in our sample tend to be hosted in early-type galaxies (Kauffmann et al. 2003b; Zhu et al. 2008). Based on these results and the discussions about the effect of star formation in §4.2, we find star formation rates in our AGN-hosting galaxies are lower.

5. Summary

Based on the sample cross-identified from Spitzer SWIRE field and SDSS spectrographic survey, we derived the formulae to calculate the stellar mass using non-linear correlations wth IRAC 3.6μ and 4.5μm luminosities. The mass-to-luminosity ratio of these two MIR luminosities are sensitive to the EW(Hα), morphology and metallicity of galaxies, especially for the former one, while the value of the EW(Hα) represents the SFH for normal galaxies. Using the g-r color to represent SFH, we re-calibrate the stellar mass formulae for various galaxies. We find these formulae are better than those which ignore the effect of SFH. We could not conclude the applicability to low metallicity galaxies due to a lack of such object in our sample, thus one must be really careful when adopting our formulae to estimate stellar masses of those galaxies. Additionally, we found that the dust emission heated by hottest young stars could enhance the IRAC 4.5 μm luminosity, especially for luminous infrared galaxies. So the formulae we derived are not applicate to these galaxies. And these formulae are also not applicate to the stronger AGNs, such as QSOs, although almost all the AGN-hosting galaxies in our sample present similar properties like absorption line galaxies (early-type), with low SFRs.

We thank the anonymous referee for constructive comments and suggestions. We acknowledge Drs. X.-Y. Xia, C.-N. Hao, Z.-G. Deng, Y. Gao, Q.-S. Gu, X.-Z. Zheng, J,-Z. Wang for advice and helpful discussions, and J.-S. Huang, Z. Wang, J.-L. Wang, and F.-S. Liu for their capable help and assistance throughout the process of *Spitzer* data reductions.

This project is supported by NSFC grants 10833006 and 10773014, and by the 973 Program grant 2007CB815406.

This work is based on observations made with the *Spitzer* Space Telescope, which is operated by Jet Propulsion Laboratory of the California Institute of Technology under NASA Contract 1407. We gratefully acknowledge University of Massachusetts and NASA/IPAC support for supply $2MASS$ data. Funding for the SDSS and SDSS-II has been provided by the Alfred P. Sloan Foundation, the Participating Institutions, the National Science Foundation, the U.S. Department of Energy, the National Aeronautics and Space Administration, the Japanese Monbukagakusho, the Max Planck Society, and the Higher Education Funding Council for England. The SDSS Web Site is http://www.sdss.org/. The SDSS is managed by the Astrophysical Research Consortium for the Participating Institutions. The Participating Institutions are the American Museum of Natural History, Astrophysical Institute Potsdam, University of Basel, University of Cambridge, Case Western Reserve University, University of Chicago, Drexel University, Fermilab, the Institute for Advanced Study, the Japan Participation Group, Johns Hopkins University, the Joint Institute for Nuclear Astrophysics, the Kavli Institute for Particle Astrophysics and Cosmology, the Korean Scientist Group, the Chinese Academy of Sciences (LAMOST), Los Alamos National Laboratory, the Max-Planck-Institute for Astronomy (MPIA), the Max-Planck-Institute for Astrophysics (MPA), New Mexico State University, Ohio State University, University of Pittsburgh, University of Portsmouth, Princeton University, the United States Naval Observatory, and the University of Washington.

REFERENCES

Baldwin, J. A., Phillips, M. M., & Terlevich, R. 1981, PASP, 93, 5B

Bell, E. F., & de Jong, R. S. 2001, ApJ, 550, 212

Bell, E. F., McIntosh, D. H., Katz, N., & Weinberg, D. 2003, ApJS, 149, 289

Bell, E. F., et al. 2005, ApJ, 625, 23

Binney, J., & Merrifield, M. 1998, Galactic Astronomy(Princeton, NJ: Princeton Univ. Press), Table 2.1

Blanton, M. R., et al. 2003, AJ, 125, 2348

Blanton, M. R., & Roweis, S. 2007, AJ, 133, 734

Brinchmann, J., & Ellis, R. S. 2000, ApJ, 536, L77

Bruzual, G., & Charlot, S. 2003, MNRAS, 344, 1000

Bruzual, G., 2007, astro-ph/0702091

Cao, C., & Wu, H. 2007, AJ, 133, 1710

Cao, C., Wu, H., Wang, Z., Ho, L. C., Huang, J. S., & Deng, Z. G. 2008, New Astronomy, 13, 16

Calzetti, D. 2001, PASP, 113, 1449

Calzetti, D., et al. 2005, ApJ, 633, 871

Calzetti, D., et al. 2007, ApJ, 666, 870

Cole, S., et al. 2001, MNRAS, 326, 255

Cutri, R. M., et al. 2003, The IRSA 2MASS All-Sky Point Source Catalog, NASA/IPAC

Daddi, E., et al. 2007, ApJ, 670, 173

Draine, B. T. 2003, ARA&A, 41, 241

Drory, N., Bender, R., & Hopp, U. 2004, ApJ, 616, L103

Elbaz, D., et al. 2007, A&A, 468, 33

Fazio, G. G., et al. 2004, ApJS, 154, 10

Finlator, K., et al. 2000, AJ, 120, 2615

Fukugita, M., et al. 1996, AJ, 111, 1748

Gallazzi, A., Charlot, S., Brinchmann, J., White, S. D. M., & Tremonti, C. A. 2005, MNRAS, 362, 41

Gallazzi, A., & Bell, E. F. 2009, astro-ph/0910.1591

Gao, J., Jiang, B. W., & Li, A. G. 2009, astro-ph/0910.3037

Gillett, F. C., Forrest, W. J., & Merrill, K. 1973, ApJ, 183,87

Helou, G., et al. 2004, ApJS, 154, 253

Huang, J.-S., et al. 2004, ApJS, 154, 44

Huang, J.-S., et al. 2007, ApJ, 664, 840

Kannappan, S. J., & Gawiser, E. 2007, ApJ, 657, L5

Kauffmann, G., & Charlot, S. 1998, MNRAS, 297, L23

Kauffmann, G., et al. 2003, MNRAS, 341, 33

Kauffmann, G., et al. 2003, MNRAS, 346, 1055

Kennicutt, R. C., Jr. 1998, ARA&A, 36, 189

Kennicutt, R. C., Jr., et al. 2003, PASP, 115, 928

Kewley, L. J., Heisler, C. A., Dopita, M. A., & Lumsden, S. 2001, ApJS, 132, 37

Kewley, L. J., Groves, B., Kauffmann, G., & Heckman, T. M. 2006, MNRAS,372,961

Kochanek, C. S., et al. 2001, ApJ, 560, 566

Léger, A., & Puget, J. L. 1984, A&A, 137, L5

Leitherer, C., et al. 1999, ApJS, 123, 3

Li, H.-N., Wu, H., Cao, C., & Zhu, Y.-N. 2007, AJ, 134, 1315

Lonsdale, C. J., et al. 2003, PASP, 115, 897

Maraston, S. T., et al. 2006, ApJ, 652, 85

Ostriker, J. P., Peebles, P. J. E., Yahil, A. 1974, ApJ, 193, 1

Pérez-González, P. G., et al. 2006, ApJ, 648, 987

Portinari, L., Sommer-Larsen, J., & Tantalo, R. 2004, MNRAS, 347, 691

Puget, J. L., & Léger, A. 1989, ARA&A, 27, 161

Rieke, G. H., et al. 2004, ApJS, 154, 25

Rix, H. W., & Rieke, M. J. 1993, ApJ, 418, 123

Roberts, M. S., & Rots, A. H. 1972, A&A, 26, 483

Rogstad, D. H., & Shostak, G. S. 1972, ApJ, 176, 315

Salim,S., et al. 2007, ApJS, 173, 267

Salpeter, E. E. 1955, ApJ, 121, 161

Skrutskie, M. F. et al. 1997, ASSL, 210, 25S

Smith, J. A., et al. 2002, AJ, 123, 2121

Strauss, M. A., et al. 2002, AJ, 124, 1810

Thuan, T. X., & Martin, G. E. 1981, ApJ, 247, 823

Tremonti, C. A., et al. 2004, ApJ, 613, 898

Veilleux, S., & Osterbrock, D. E. 1987, ApJS, 63, 295

Wen, X.-Q., Wu, H., Cao, C., Xia, X.-Y. 2007, Chinese Journal of Astronomy and Astrophysics, 7, 187

Werner, M. W., et al. 2004, ApJS, 154, 1

Willner, S. P., Soifer, B. T., Russell, R. W., Joyce, R. R., & Gillett, F. C. 1977, ApJ, 217, 121

Wu, H., Zou, Z. L., Xia, X. Y., & Deng, Z. G. 1998, A&AS, 132, 181

Wu, H., Cao, C., Hao, C.-N., Liu, F.-S., Wang, J.-L., Xia, X.-Y., Deng, Z.-G., & Young, C. K. S. 2005, ApJ, 632, L79

Wu, H., Zhu, Y. N., Cao, C., & Qin, B. 2007, ApJ, 668, 87

York, D. G., et al. 2000, AJ, 120, 1579

Zhu, Y. N., Wu, H., Cao, C., & Li, H. N. 2008, ApJ, 686, 520

This preprint was prepared with the AAS LaTeX macros v5.2.

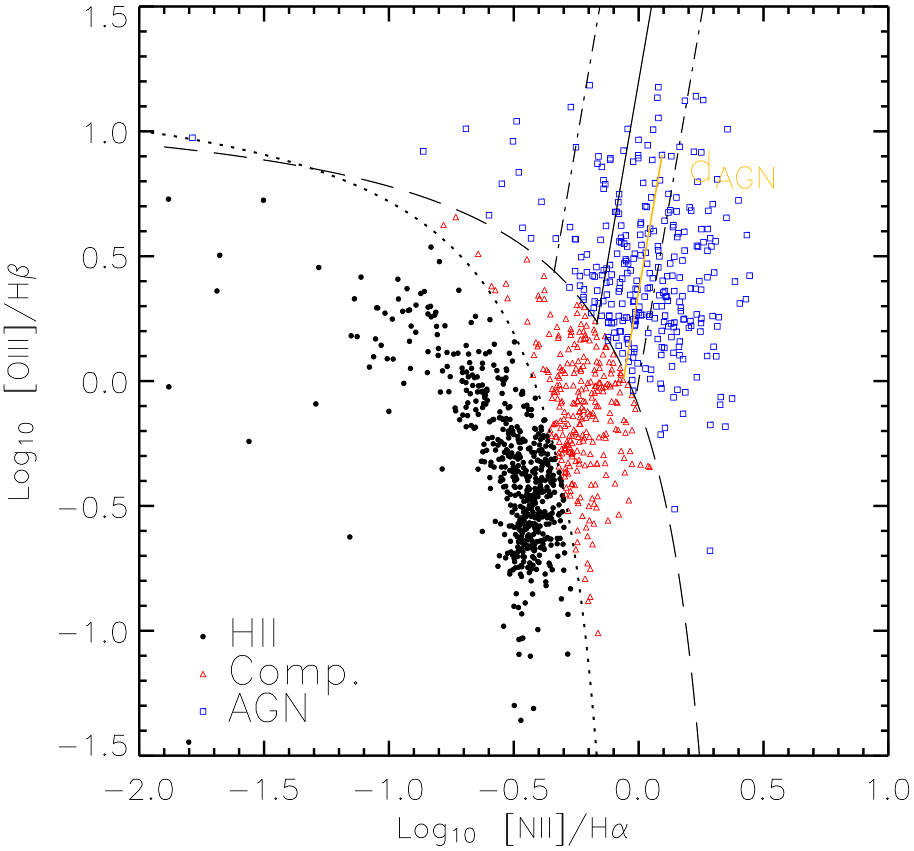

Fig. 1.— The BPT diagnostic diagram: [NII]/Hα vs [OIII]/Hβ. The criteria from Kauffmann et al. (2003b) and Kewley et al. (2001) are illustrated as dotted and dashed curves, respectively. The objects below the dotted curve are defined as star-forming galaxies. The triangles between the above two curves are those classified as composite galaxies, while the boxes above the dashed curve denote AGNs. We use the distance d_{AGN}, which was defined by Wu et al. (2007), to characterize AGN activity. The two dotted-dashed lines mark the boundaries that were used by Wu et al. (2007). An example was show in this figure with orange solid line.

Fig. 2.— Comparing the referenced stellar mass, which derived by photometries fitting, with those from spectral features fitting supplied by MPA/JHU (Panel (a)) for about eighty thousand galaxies randomly selected from SDSS DR4. In Panel (b), the comparing between the reference and the stellar mass computed based on the rest-frame g-r color, r band model magnitude and the equation by Bell et al. (2003) is presented. Please note that a factor of 0.15 was adding to the equation of Bell et al. (2003) to correct the 'diet Salpeter' IMF to the normal Salpeter (Salpeter 1955) IMF.

Fig. 3.— The correlations between the stellar mass ratio and the referenced stellar mass (a), *g*-*r* color for about eighty thousand galaxies randomly selected from SDSS DR4. The stellar mass ratio represent the discrepancies between the referenced stellar mass and the stellar mass estimated based on the rest-frame *g*-*r* color, *r* band model magnitude and the equation by Bell et al. (2003) is presented. Same as in Figure 2, a factor of 0.15 was adding to the equation of Bell et al. (2003) to correct the 'diet Salpeter' IMF to the normal Salpeter (Salpeter 1955) IMF.

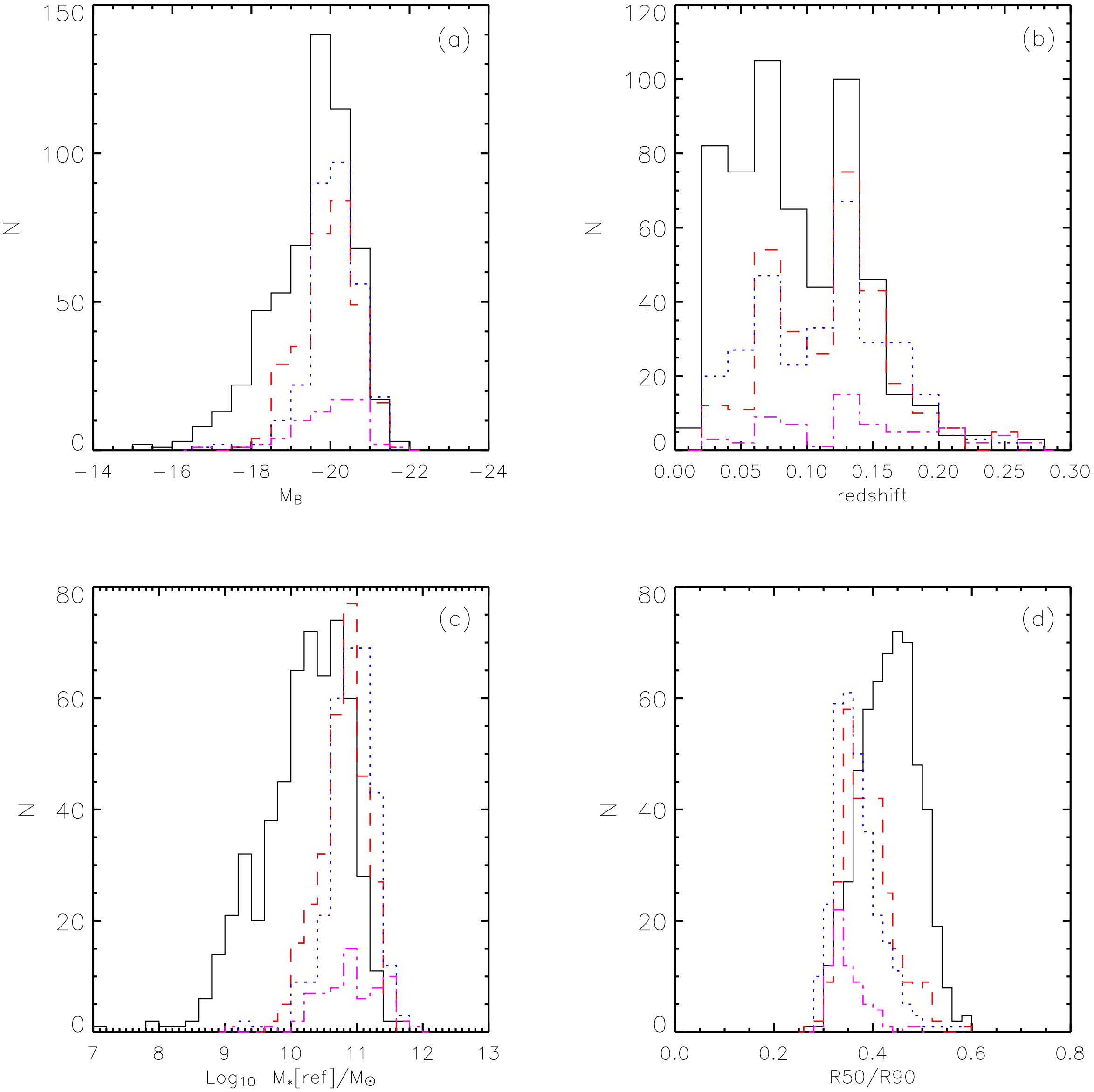

Fig. 4.— The distributions of (a) absolute B-band magnitude; (b) redshift; (c) the referenced stellar mass; (d) the concentration parameters ($R50/R90$) for star forming galaxies (black solid lines), composites (red dashed lines), AGNs (blue dotted lines) and absorption line galaxies (pink dashed-dotted lines).

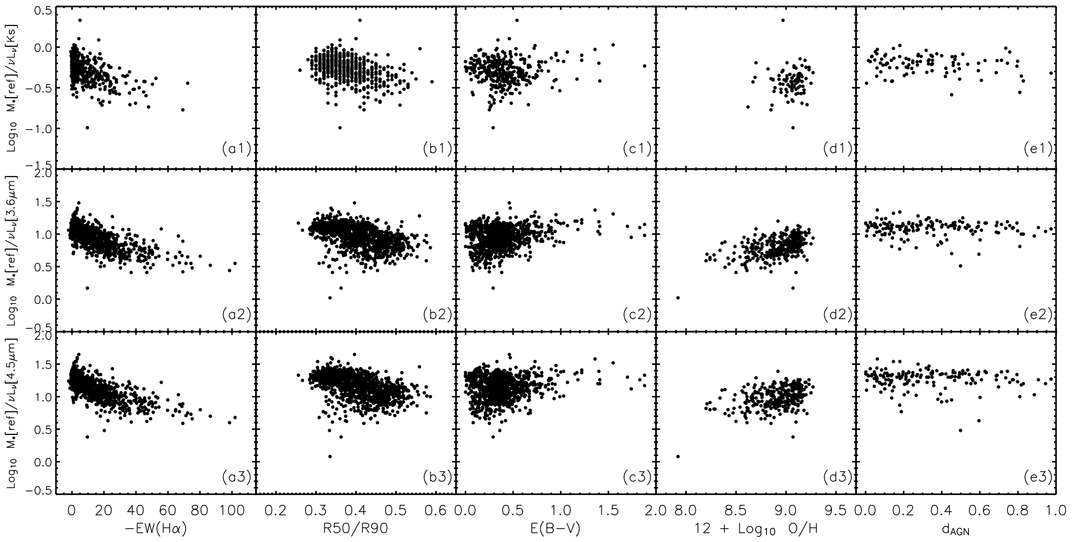

Fig. 5.— Comparing the mass-to-luminosity ratios with various factors, include Hα equivalent width (a1, a2, a3), $R50/R90$ (b1, b2, b3), intrinsic reddening (c1, c2, c3), oxygen metallicity (d1, d2, d3) and the activity of AGN (e1, e2, e3). The $2MASS$ K_s band luminosity is used in upper five panels. The 3.6μm luminosity is used in middle five panels. The 4.5μm luminosity is used in the bottom five panels.

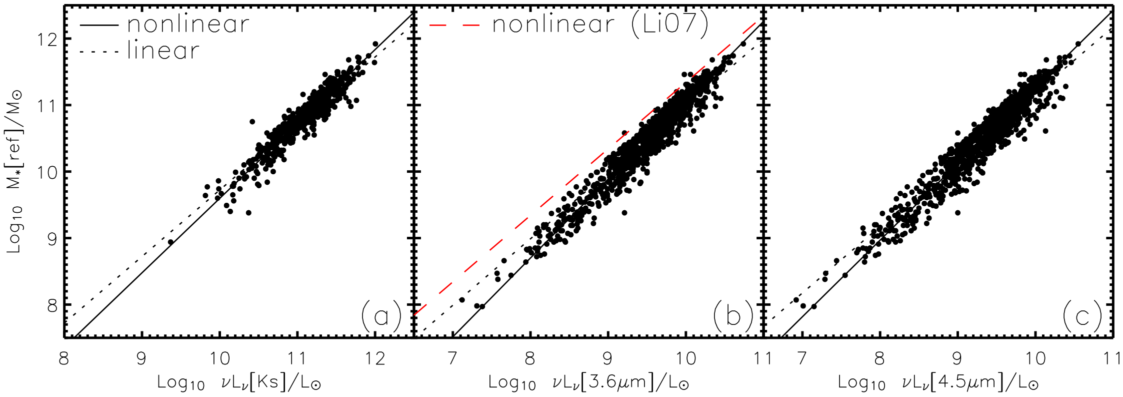

Fig. 6.— Correlations between referenced stellar mass and 2*MASS* K_s band, two IRAC bands luminosities for all the galaxies. The best nonlinear and linear fits are illustrated as solid and dotted lines. The red dashed lines show in Panels (b) represent the nonlinear fits for more than one hundred luminous SWIRE-field galaxies by Li et al. (2007).

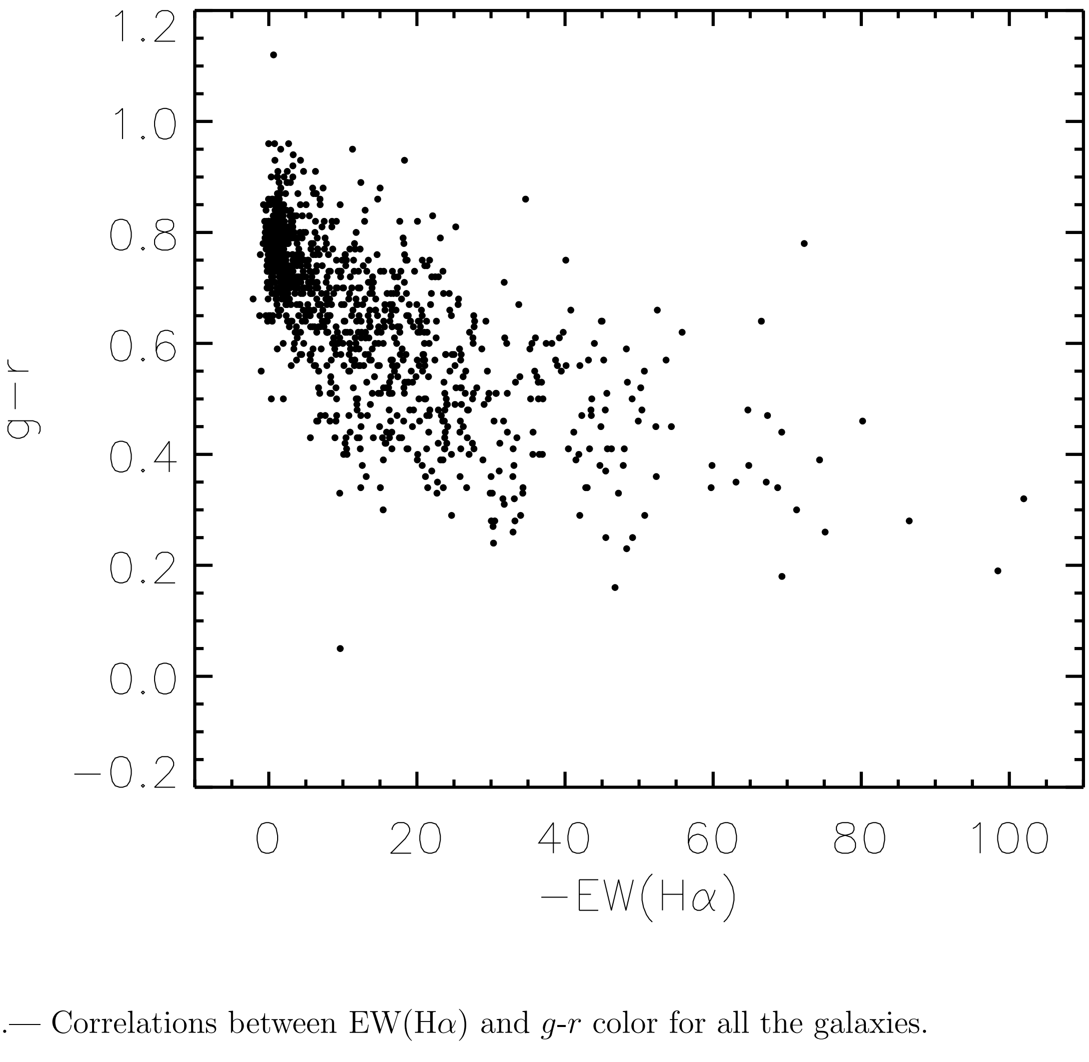

Fig. 7.— Correlations between EW(Hα) and g-r color for all the galaxies.

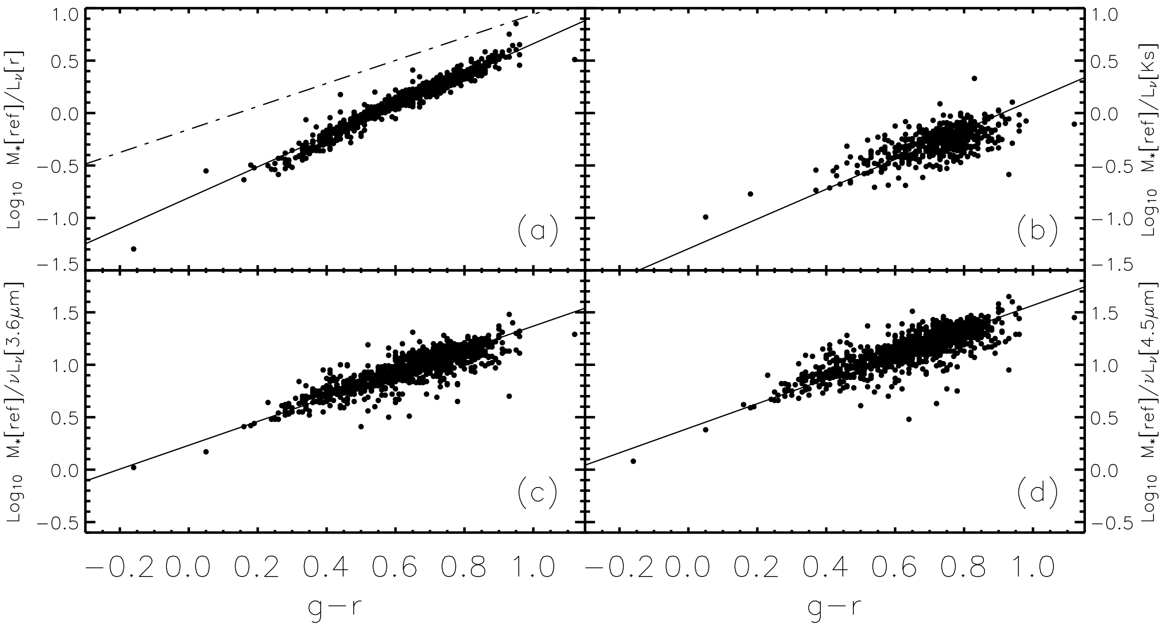

Fig. 8.— Correlations between *g*-*r* color and various mass-to-luminosity ratios for all the galaxies. Due to the relatively lower sensitivity in 2*MASS* K_s band observation, only 544 galaxies were detected and presented in Panel (b). The solid lines represent the best nonlinear fits. The dotted-dashed line in Panel (a) is the respective line by Bell et al. (2003).

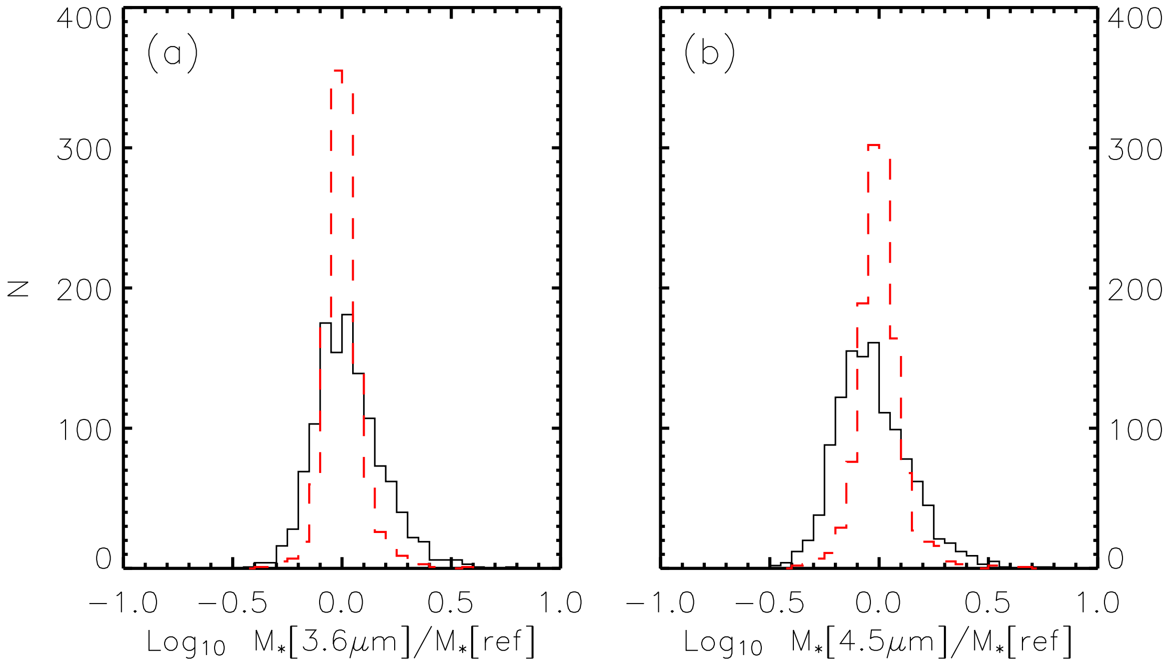

Fig. 9.— The distributions of ratios of the derived stellar masses divided by the referenced ones. The derived stellar masses were computed based on Eq.2 (black solid lines in Panel (a)), Eq.6 (red dashed lines in Panel (a)), Eq.3 (black solid lines in Panel (b)), Eq.7 (red dashed lines in Panel (b))

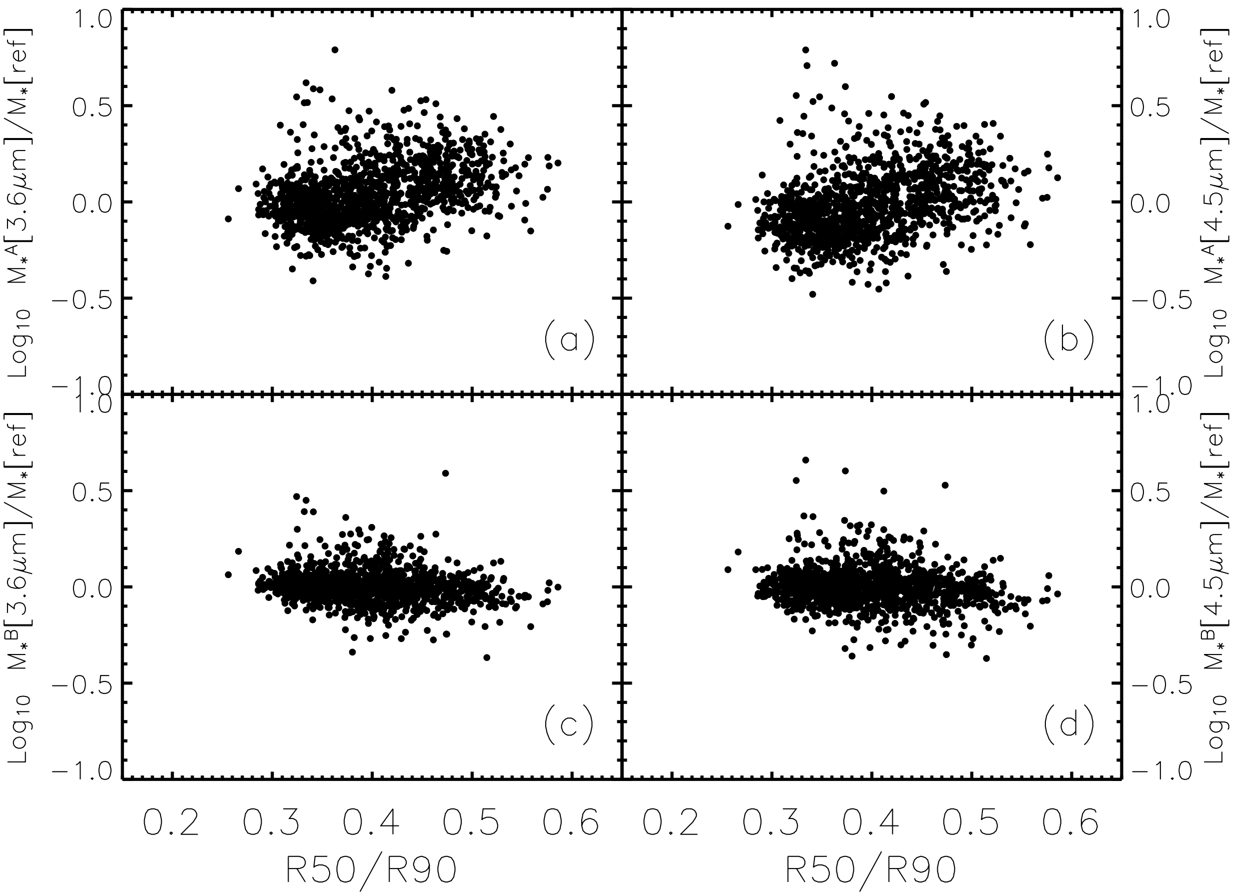

Fig. 10.— Correlations between concentration parameters and the stellar mass ratios, which are the discrepancies between the stellar mass derived from our calibrated formulae and the reference. The derived stellar mass by using Eq.2, 3, 6, 7 is shown in Panel (a), (b), (c), (d), respectively.

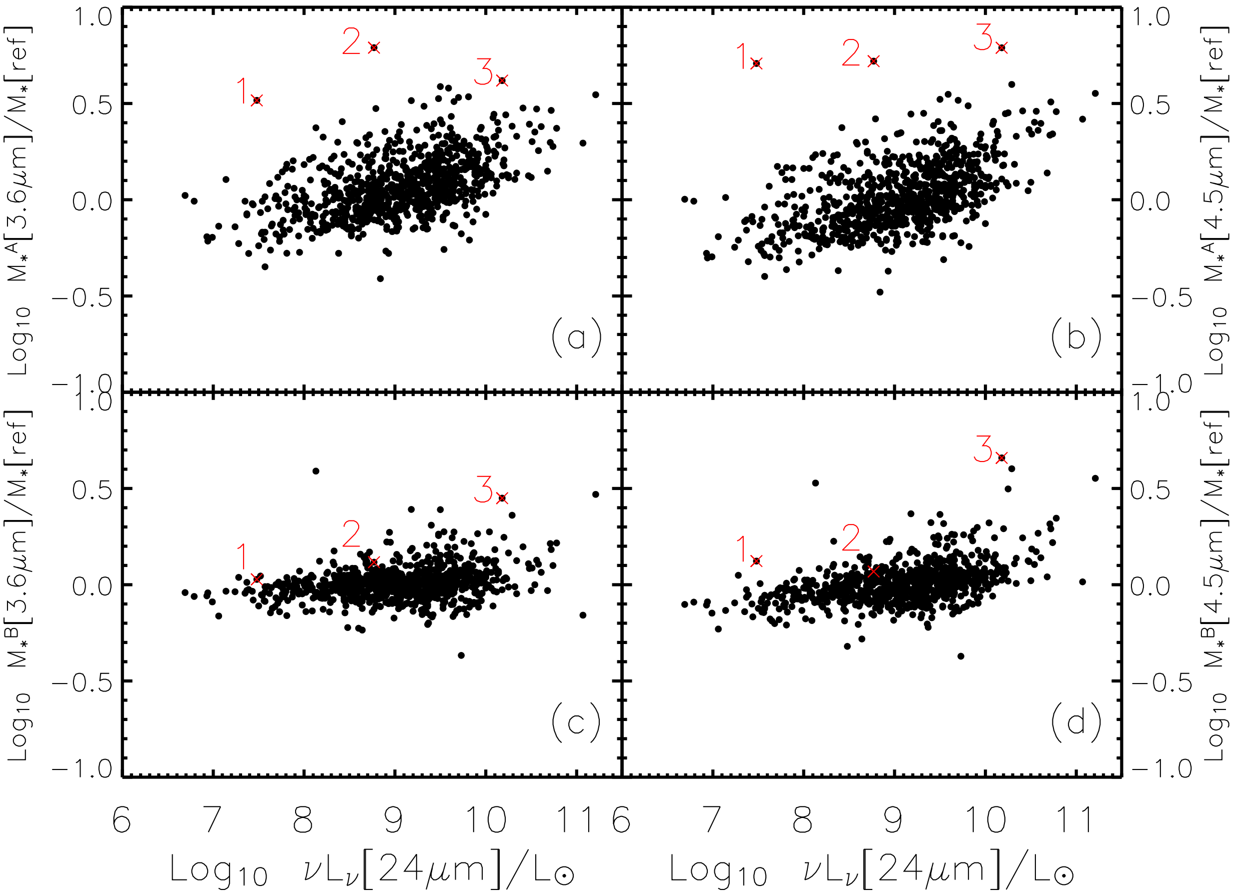

Fig. 11.— Similar as Figure 10, but the concentration parameters were instead of 24μm luminosities. The red crosses represent the three scatters, and they were signed out with numbers.

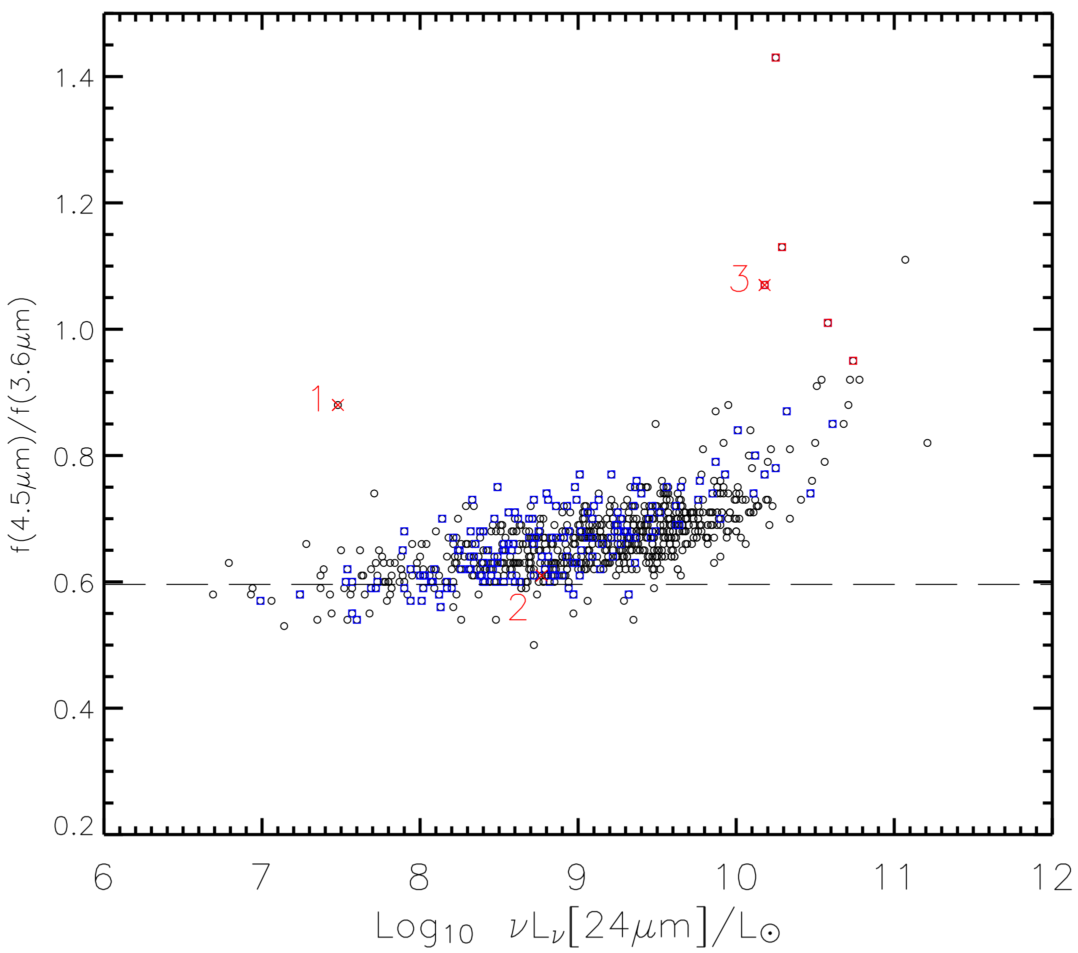

Fig. 12.— Correlations between 24μm luminosity and the flux ratio between 3.6μm and 4.5μm for all the galaxies. The blue boxes represent AGNs. The red boxes represent AGNs with 3.6μm-to-4.5μm ratio larger than 0.9. The three outliers in Figure 11 were sighed out with red crosses. The dashed line represent the factor of 0.596 which is the ratio between 4.5μm and 3.6μm flux by (Helou et al. 2004) with the assumption that the entire IRAC 3.6μm and 4.5μm band luminosities are from the stellar emission.

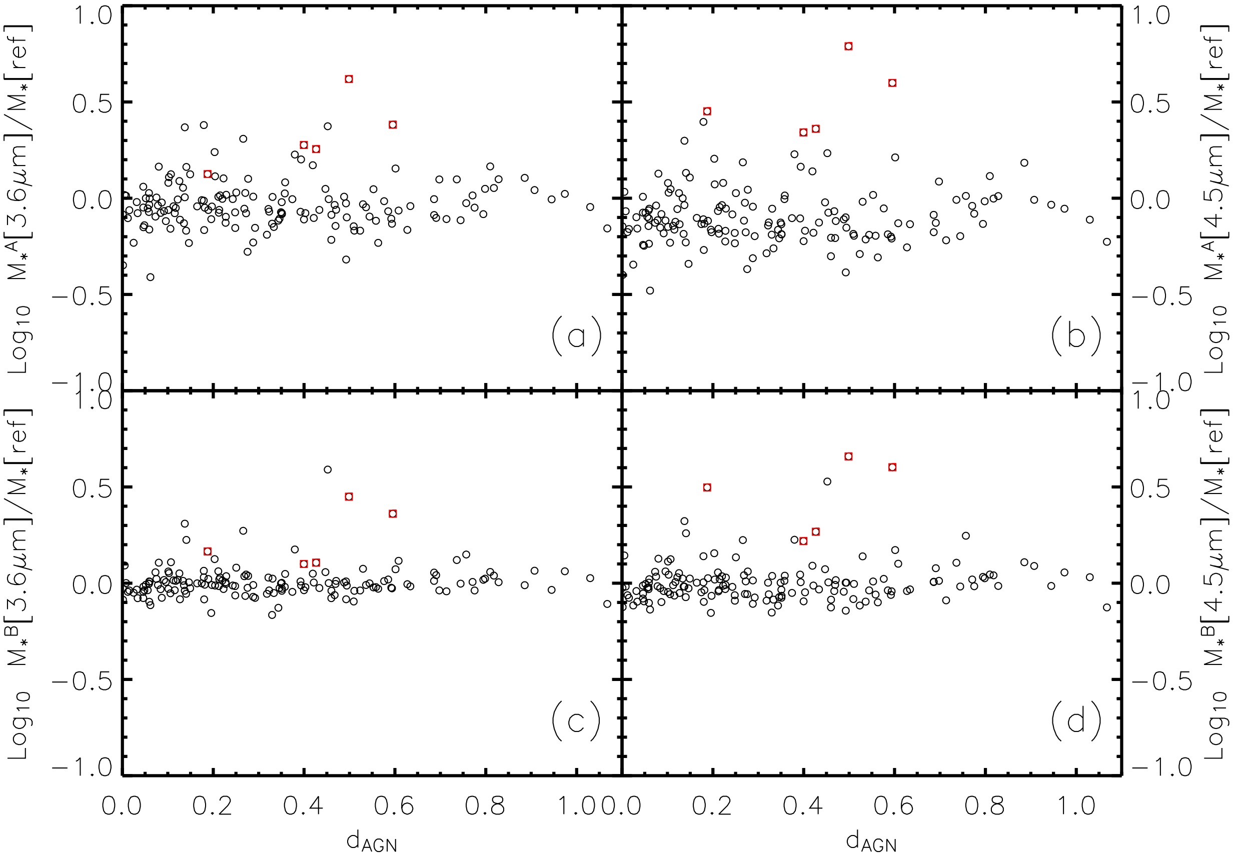

Fig. 13.— Correlations between AGN activity and the stellar mass ratios, which are the discrepancies between the stellar mass derived from our calibrated formulae and the reference. Here, the distance d_{AGN}, which was defined by Wu et al. (2007), to characterize AGN activity. The derived stellar mass by using Eq.2, 3, 6, 7 is shown in Panel (a), (b), (c), (d), respectively. The red boxes represent the respective AGNs in Figure 12 with higher 4.5μm-to-3.6μm flux ratio (large than 0.9).

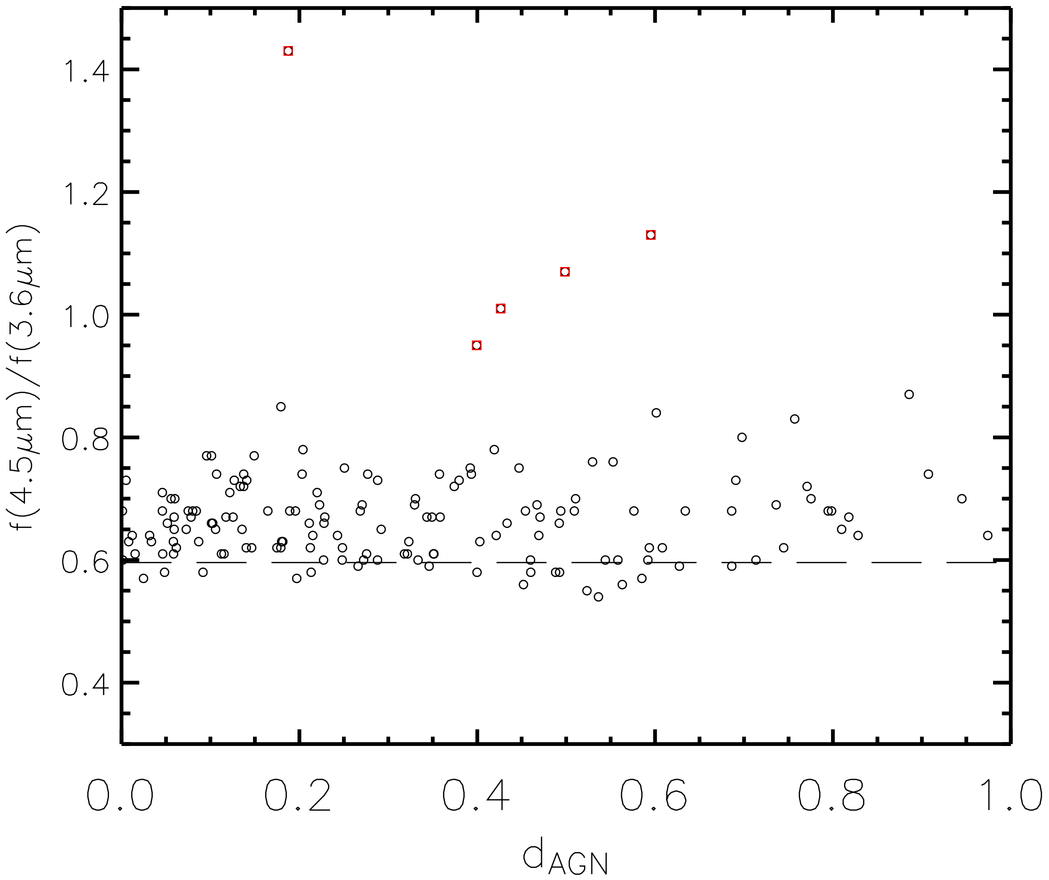

Fig. 14.— Correlations between the distance d_{AGN}, which represent AGN activity, and the flux ratio between 3.6μm and 4.5μm for AGNs. The red boxes represent the sources with 4.5μm-to-3.6μm flux ratio large than 0.9. The dashed line represent the factor of 0.596 such as plotted in Figure 12.

Table 1. Correlations coefficients between stellar mass and $K_{\rm s}$ band, 3.6μm and 4.5μm luminosities

y (1)	x (2)	a (3)	b (4)	s (5)	r (6)	c (7)	N (8)
M_*	$\nu L_\nu[K_{\rm s}]$	– 1.60±0.05	1.12±0.02	0.10	0.94	0.28±0.11	544
M_*	$\nu L_\nu[3.6\mu m]$	– 0.79±0.03	1.19±0.01	0.11	0.96	0.99±0.14	1220
M_*	$\nu L_\nu[4.5\mu m]$	– 0.25±0.03	1.15±0.01	0.12	0.95	1.17±0.14	1220

Note. — Col.(1): the referenced stellar mass in solar unit; Col.(2): names of MIR luminosities; Col.(3)-(4): the coefficients a and b of the nonlinear fit: $\log_{10}(y)$ =a+b$\log_{10}(x)$; Col.(5): the standard deviation s of the fitting residuals; Col.(6): the coefficient r of the Spearman Rank-order correlation analysis; Col.(7): the coefficient c of the linear fit: $\log_{10}(y)$ =c+ $\log_{10}(x)$; Col.(8): the number of sample galaxies used for the fitting procedures.

Table 2. Correlations of M_*/L and colors

y (1)	x (2)	a (3)	b (4)	s (5)	r (6)	N (7)
$M_*/L_\nu(r)$	$g-r$	-0.81 ± 0.01	1.47 ± 0.01	0.03	0.97	1215
$M_*/L_\nu(K_\mathrm{s})$	$g-r$	-1.29 ± 0.05	1.42 ± 0.06	0.08	0.54	410
$M_*/\nu L_\nu[3.6\mu m]$	$g-r$	0.23 ± 0.01	1.14 ± 0.01	0.05	0.83	1210
$M_*/\nu L_\nu[4.5\mu m]$	$g-r$	0.39 ± 0.01	1.17 ± 0.02	0.06	0.80	1208

Note. — Col.(1): various mass-to-luminosity ratios in solar unit; Col.(2): *g*-*r* color; Col.(3)-(4): the coefficients a and b of the nonlinear fit: $\log_{10}(y)$ =a+b$\log_{10}(x)$; Col.(5): the standard deviation s of the fitting residuals; Col.(6): the coefficient r of the Spearman Rank-order correlation analysis; Col.(7): the number of galaxies used for the fitting procedures.